Low temperature dependence of electrical resistivity in obliquely sputter-deposited transition metal thin films

Hamidreza Gerami [1], Jean-Marc Cote [2], Antonio Jesús Santos [3, 4], and Nicolas Martin [2 *]

[1] Université de Franche-Comté, CNRS, Institut FEMTO-ST, F-25000 Besançon Cedex, France

[2] SUPMICROTECH, CNRS, Institut FEMTO-ST, F-25000 Besançon Cedex, France

[3] IMEYMAT: Institute of Research and Electron Microscopy of Materials of the University of Cadiz, E-11510 Puerto Real, Spain

[4] Department of Materials Science and Metallurgic Engineering, and Inorganic Chemistry, Faculty of Sciences, University of Cádiz, E-11510 Puerto Real, Spain

* Corresponding author: nicolas.martin@femto-st.fr

Highlights

- Hcp and bcc transition metal thin films are sputtered by oblique angle deposition.
- Tilted columnar architecture is favored increasing deposition angles from 0 to 85°.
- Resistivity at low temperature reveals electron-phonon-defect interactions.
- Deposition angle influences electron-phonon-defect interference effect.

Graphical abstract

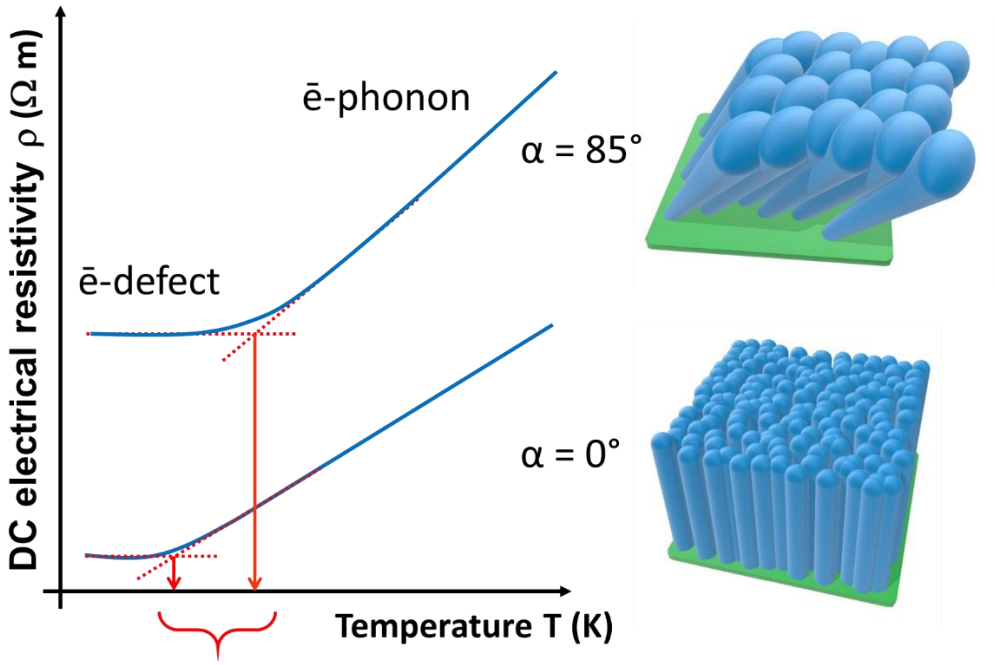

Shift of the crossover temperature related to the ē-phonon-defect interference effect

Abstract

Transition metals exhibiting hcp (Ti, Zr, Hf) and bcc (V, Nb, Ta, Cr, Mo, W) crystalline structures are DC sputter-deposited by oblique angle deposition. A constant film thickness of 400 nm is prepared, whereas the deposition angle α is systematically changed from 0 to 85°. A columnar structure is produced with column angle reaching β = 50° for the highest deposition angle. Crystallinity and grain size are both reduced with an increasing deposition angle, especially for α higher than 60°. DC electrical resistivity *vs.* temperature in the range 7-300 K shows a typical metallic-like behavior with films becoming more resistive for high deposition angles. For temperatures higher than 100 K, the linear temperature dependence of resistivity is obtained for films prepared with deposition angles lower than 60°. The electron-phonon is the main interaction acting on electronic transport mechanism. Oblique deposition angles give rise to an enhancement of electron-phonon interactions with a saturation effect of electrical resistivity for some metals. Resistivity measurements at low temperatures (down to 7 K) show the predominance of electron-defect interactions. Electron-phonon-defect interaction effect is particularly investigated as a function of the deposition angle and a shift of the crossover temperature is brought to the fore.

Keywords

Transition Metals, Oblique Angle Deposition, Resistivity, Tilted columns, Electron-phonon-defect interactions.

1. Introduction

Electronic transport properties of bulk metals at very low temperature have been thoroughly and deeply investigated in solid-state physics. Many studies are based-on the temperature dependence of DC electrical resistivity, especially when measurements are performed for thin film materials at very low temperature [1-3]. Numerous investigations clearly showed that electron-phonon interactions are strongly modified when disordered metallic films are produced [4-6]. Such interactions are typically illustrated by a linear evolution of resistivity *vs.* temperature for a range exceeding a few tens of K. On the other hand, electron-defect interactions prevail as the temperature decreases and reaches a few K since resistivity becomes constant. This transition corresponds to variations of resistivity with a temperature dependency following a power law. Interferences between electron-phonon and electron-defect interactions turn out to be significant for a temperature range closely connected to the Debye temperature θ (about $\theta/10$). As a result, a crossover temperature can be defined, the latter being strongly influenced by the long-range order in the metal and by the concentration of defects [7, 8].

Although the resistivity *vs.* temperature evolution is well known for bulk transition metals, it may exhibit some original behaviors when compounds are prepared as thin films, particularly when the thickness is in the nanometric range [9]. In addition, the temperature dependence of resistivity may be completely disturbed by structural defects, impurities, grain size and last but not least, by the architecture of the films, especially the structure at the nanometric scale [10, 11]. The fractal dimension (wires, monolayers), the porous structure, or the chemical composition strongly influence the scattering phenomenon of electrons and thus the electronic transport in thin films [12-14]. In order to tune the architecture and design of coatings, some original and convenient deposition strategies give rise to unconventional

structuring of metallic thin films produced by vacuum processes (e.g., evaporation, sputtering …). Among these deposition techniques, one has recently been developed as a powerful approach: the oblique angle deposition (OAD) for fabricating tilted columns, zigzags or even spiral structures, among others. This OAD method plays only with the deposition angle α and/or the substrate rotation φ during the deposition stage. It allows structuration of metallic, semiconducting and insulating thin films at the nanometric scale, leading to the production of porosity-controlled films, which exhibit some extended physical properties [15-18]. Experimental as well as theoretical studies have ever reported on the temperature dependence of resistivity in OAD films. However, most of them have been focused on temperatures higher than the room temperature [19-22]. A few studies have been devoted to the cryogenic or the very low temperature range [23, 24]. Therefore, the role of crystalline structure, deposition angle and columnar architecture typically obtained in OAD films on the electron scattering phenomenon, particularly electron-phonon-defect interactions, has never been reported for nanostructured metallic thin films prepared by means of the sputtering process.

In this article, we report on electronic transport properties of tilted columnar transition metal thin films sputter-deposited by OAD. Hcp (Ti, Zr, Hf) and bcc (V, Nb, Ta, Cr, Mo, W) transition metals are mainly investigated. DC electrical resistivity *vs.* temperature is systematically measured in a temperature range, which allows understanding the electron-phonon-defect interactions, i.e., for temperatures much lower than the Debye temperature of each metal. The type of metal as wells as the voided morphology of the tilted columnar structure are examined, and the influence of the deposition angle on the crossover temperature corresponding to the interferences between electron-phonon and electron-defect interactions is particularly discussed.

2. Experimental section

Ti, V, Cr, Zr, Nb, Mo, Hf, Ta and W thin films were deposited on glass and (100) silicon substrates from pure metallic targets (99.95 % of purity and 51 mm diameter) in the same DC magnetron sputtering system (previously described in [17]). Briefly, this system was a 40 L homemade vacuum chamber evacuated with a turbomolecular pump backed with a primary pump leading to a base pressure below 10^{-5} Pa. The distance between the center of the substrate and that of the target was 65 mm. All targets were sputtered in a pure argon atmosphere with a flow rate of 2.6 sccm and a constant pumping speed of 13 L s^{-1} giving rise to an argon sputtering pressure of 0.3 Pa. The target current was fixed at 200 mA for all targets. Substrates were grounded during all runs with no external heating. They were ultrasonically cleaned with acetone and ethanol before thin films deposition. The deposition angle α was gradually changed using the following angles: 0, 30, 60, 70, 80 and 85°. The deposition time was adjusted to obtain the same film thickness (measured with a profilometer) of 400 nm for every deposition angle. Since substrates are inclined during the oblique angle deposition process, thickness of the films (following the direction perpendicular to the particle flux) becomes intrinsically inhomogeneous and a gradient appears. Such a gradient from one side of the sample to the other one becomes even more significant as the deposition angle rises. In order to minimize this effect, we focus only on a small area surface for each sample (center of the substrate), i.e., around 5×5 mm^2. In this way, one can assume that the films thickness is quite homogeneous (difference of a few % of the 400 nm average thickness).

Structural analyses were carried out for films deposited on silicon substrates. The morphology was studied using a scanning electron microscope (SEM) JEOL JSM 7600F to observe the surface and cross-section of the films. The crystallographic structure was determined by X-ray diffraction (XRD) technique. Measurements were performed using a

PAnalytical Aeris diffractometer with a copper X-ray source (Cu $\lambda_{K\alpha1,2}$ = 0.15418 nm) following the grazing incidence configuration (GIXRD) using an X-ray incidence angle θ = 0.8°. Scans were performed with 2θ angle from 20° to 90° with a step of 0.02° per 1 s. The DC electrical resistivity measurements were carried out from 7 to 300 K for films deposited on glass substrates using the four-probe van der Pauw method. A cryostat system from Advanced Research Systems Incorporation (ARS cryocooler series CS-204-AE) was used to reduce the sample temperature down to about 6 K in a chamber equipped with a pumping units leading to a vacuum below 10^{-4} Pa. A temperature ramp of 1 K min^{-1} was applied for all resistivity measurements.

3. Results and discussion

Using the conventional sputtering process (i.e., with a deposition angle α = 0°) leads to the growth of thin films. They exhibit a typical dense and columnar structure, as shown in Fig. 1 from the SEM top and cross-section views of Zr, Ta and Cr films (for clarity, SEM pictures for the other metals are not shown here but in the Supplementary Material Section III). These 3 metals are only presented in the article to illustrate results obtained for one bcc metal of group 6 and period 4 (i.e., Cr), one bcc metal of group 5 and period 6 (i.e., Ta), and one hcp metal of group 4 and period 5 (i.e., Zr). As a result, these 3 metals are representative of 3 different groups and 3 different periods.

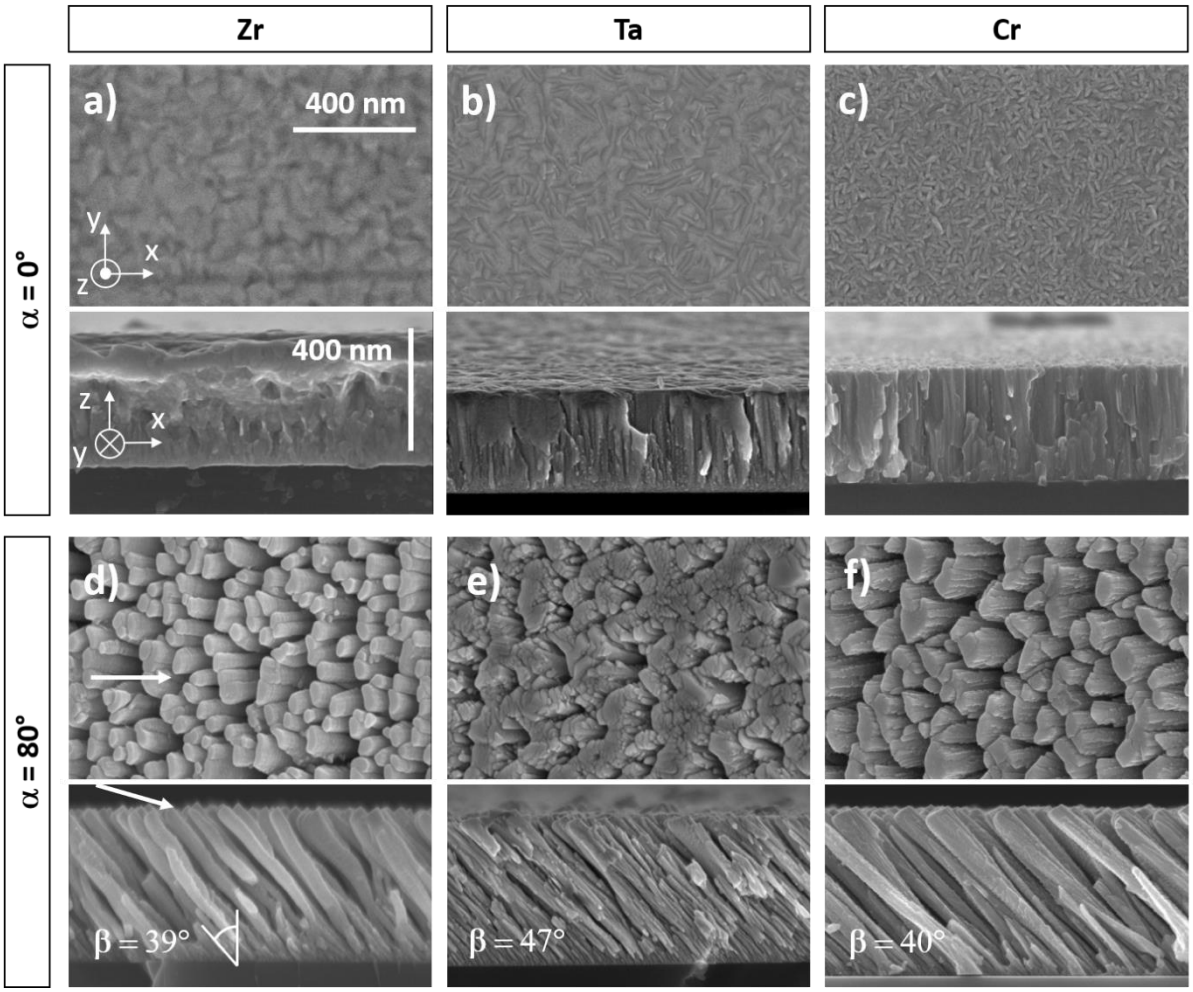

Figure 1: Top and cross-section SEM views of Zr, Ta and Cr films sputter-deposited: a), b) and c) by conventional sputtering (α = 0°); d), e) and f) by oblique angle deposition with a deposition angle α = 80°. White arrows indicate the direction of the incoming particle flux. The column angle β is also specified for the tilted columnar architectures.

The sputtering pressure involved during the deposition process is quite low (0.3 Pa) combined with a target-to-substrate distance of 65 mm. For such operating conditions, sputtered particles are mainly in a ballistic regime. Since DC sputtering mode is implemented with a grounded substrate, it can be first assumed that no ions impinge on the growing film and the normalized energy related to heating effects caused by kinetic energy of sputtered particles is low [25]. In

addition, no external heating has been used during the deposition stage. Therefore, the homologous temperature defined as the film growth temperature-to-the melting temperature ratio is below 0.15, which corresponds to the typical zone 1 of the structure zone model. For such operating conditions, one can expect densely packed fibrous grains for all the nine transition metals of this study. Top view of as-deposited metallic films with $\alpha = 0°$ all exhibit a randomized surface-orientation of the column apexes. For such operating conditions, the islands expand during deposition allowing neighboring columns to contact and coalesce. A fine and tightly packed columnar microstructure develops, which is clearly illustrated for all metals from the cross-sections view (Fig. 1a, b and c).

Increasing the deposition angle α above glancing values (i.e., $\alpha > 70°$) leads to a tilted columnar architecture for all metallic films as shown from the cross-section views in Fig. 1d, e and f. The column angle β reaches 35 to 50° for films sputter-deposited with $\alpha = 85°$ and an argon pressure corresponding to the ballistic regime of sputtered particles [26]. For these glancing angle conditions, the atomic shadowing effect is particularly exacerbated and a distinct porous architecture is clearly produced with voided between columns. Such a shadowing effect correspondingly leads to the growth of self-affine columnar nanorods with tilting angle depending on the nature of sputtered metals but especially on operating conditions. High-aspect-ratio rods are obtained since deposition was performed at room temperature and melting point of all studied metals is high (especially for hcp and fcc metals), which gives rise to a low homologous growth temperature (i.e., below 0.15 as previously noticed).

It is also worth noticing that the broadening effect of the columns tends to become stable for Zr films as the thickness increases, whereas it still rises for Ta and Cr films. In addition, Zr columns appear more independent to each other, while for the other metals, column bundles clearly appear in the direction perpendicular to the particle flux. Mareus *et al.* [27] recently

showed for TiN GLAD thin films the effect of surface diffusion processes on the column tilt angle and their ability to form bundles following the direction perpendicular to the particle flux. These dissimilar features of morphological structure between Zr and Ta or Cr films are mainly connected to the different surface diffusion of deposited materials. For hcp metals like those of this study (Ti, Zr and Hf), self-diffusion coefficients and activation energies are systematically lower than that of bcc metals (V, Nb, Ta, Cr, Mo and W) leading to shorter diffusion lengths [28]. As a result, columns produced for hcp metals with the highest deposition angles rather exhibit an independent columnar growth disconnected to each other with a quite regular elliptical cross-section as shown in Fig. 1d. Bcc metals show columns with an enhanced transverse growth leading to a less defined intercolumn separation with an asymmetric and wide cross-section in the direction perpendicular to the flux. A crescent-like shape is rather observed from the apex of the columns (Fig. 1e and f) with a significant bundling and so, a fanning and chaining effect of the columnar architecture.

Since all films were produced without any external heating (i.e., homologous temperature lower than 0.15), one can expect poorly crystallized hcp and bcc metals. However, XRD patterns recorded at grazing angle show a film crystallinity significantly influenced by the deposition angle (Fig. 2). With a conventional sputtering process ($\alpha = 0°$), intense diffracted signals are commonly recorded for all transition metals sputter-deposited on Si substrate. As expected, patterns well correspond to the hcp phase for Ti, Zr and Hf metals, and bcc phase for V, Nb, Ta, Cr, Mo and W metals with no clear preferential orientation (to see Supplementary Material Section I for all transition metal thin films prepared with different depositions angles).

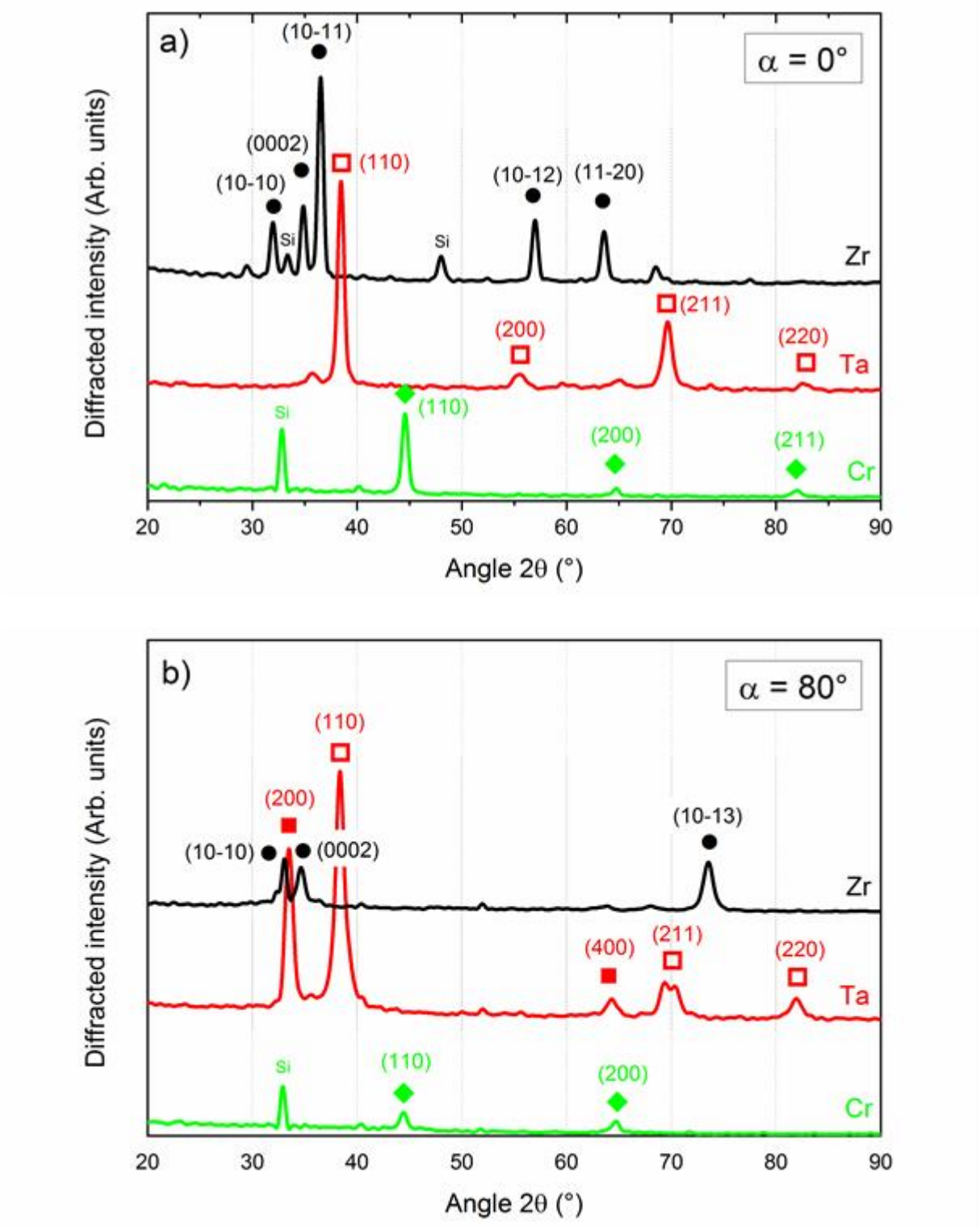

Figure 2: Grazing incidence X-ray diffraction patterns of Zr, Ta and Cr films prepared a) by conventional sputtering (α = 0°), and b) by oblique angle deposition with a deposition angle α = 80°. ● = hcp Zr phase; □ = bcc α-Ta phase; ■ = A15 β-Ta phase; ◆ = bcc Cr phase.

Increasing the deposition angle systematically reduces the peaks intensity and favors their widening. For films prepared with a deposition angle α = 85°, diffracted signals are strongly diminished and some peaks even disappear. It is also interesting of remarking that other peaks appear, particularly for Ta and W films prepared with $\alpha > 60°$. They correspond to the metastable A15 β-phase of the metal. Former studies reported that a substantial oxygen concentration in bcc metallic films such as Ta, W or even Cr, promotes the stability of the β-phase [29]. In addition, films grown with low-energy atomic flux onto substrates at temperatures below 400°C also produce a significant amount of this β-phase. Therefore, assuming that higher deposition angles induce the formation of intercolumn voids [30], oxygen occurrence as well as glancing angle deposition favor the formation of such metastable compounds. Oxygen concentration has been measured for some metals (not shown here). For all metals that we studied, this oxygen concentration can reach about 5 to 10 at.% for the highest deposition angles (higher than 70°) and the highest reactive metals (Ti, W or Ta), without showing a clear trend as a function of the deposition angle. For other elements like Cr, V, Nb, Zr or Hf, the amount of oxygen was not significant (lower than a few at. %) and so no clear conclusions can be drawn. As a result, some metallic films (W and Ta, particularly) prepared with glancing deposition angles (and so extreme shadowing conditions) give rise to a mixture of α and β phases. A growing amount of the β phase is then obtained with a nanocrystalline size, as clearly shown from XRD results (Fig. 2b).

Lowering and widening the diffracted intensity means a reduction of the long-range order in the films, especially for deposition angles higher than about 60-70°. This range of angles has been reported as a critical value for many materials [31] and correlates with the shadowing effect becoming prevalent. A more porous columnar architecture, combined to a

high concentration of structural defects, is then produced during the growth, which enhances the sensitivity of the film to impurities, particularly when the metal is reactive towards oxygen. Most of oxide compounds are formed on the surrounding parts of the columns or at the film/substrate interface. These oxides are mainly amorphous or poorly crystallized [32]. Thus, no signals can be seen from XRD. However, metals like W or Ta may produce the A15 phase as shown in Fig. 2b or in Section I of Supplementary Material for W films when deposition angle increases. Crystal growth is then disturbed and their size reduced for glancing deposition angles as illustrated for Cr, Ta and Zr films in Fig. 3 (for clarity, crystal size for the other metals are not shown). For each metal, the Scherrer's law has been applied on the most intense diffracted signal (only for the α-phase for metals exhibiting a α+β phase mixture). Up to a deposition angle of 60°, the crystal size L remains unchanged in-between 10-20 nm for all sputter-deposited metals. One does not expect films with a long-range crystalline order since depositions have been performed without any external heating and because of the low homologous temperature for all films (growth temperature-to-melting temperature ratio is always below 0.15). Crystal size is significantly reduced for high glancing angles and can be lower than a few nanometers when α reaches 85°.

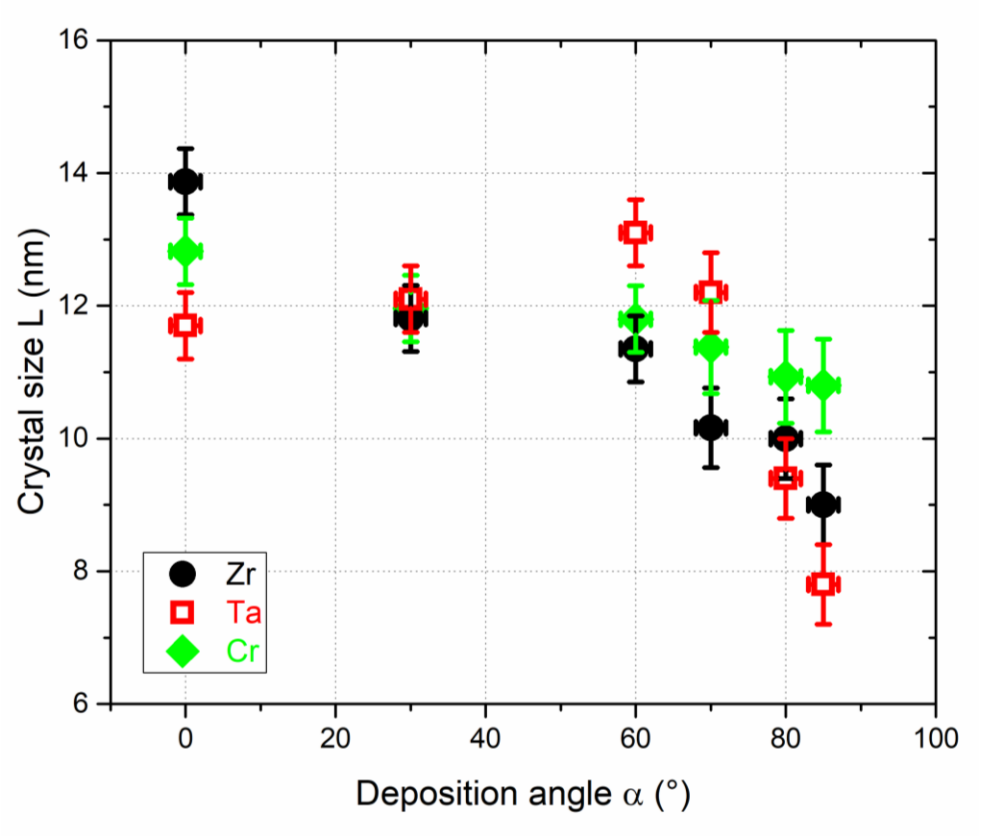

Figure 3: Evolution of the crystal size L (Scherrer's law applied for the most intense peak obtained from XRD patterns) as a function of the deposition angle α for Zr, Ta and Cr films.

Although crystalline growth of GLAD thin films is not fully understood due to some complex mechanisms induced by the oriented vapor flux (e.g., development of a biaxial texture [33], preferential crystallographic orientation and stress relaxation [34], in-plane alignment [35], and so on), this crystal size reduction has ever been reported from others for the deposition of metals and ceramics [36, 37]. It is mainly assigned to a decrease of the energy per incident atom. Rising the deposition angle favors the proportion of thermalized sputtered particles impinging on the growing film compared to the ballistic ones. This decrease of crystallinity also correlates with variations of morphology and porosity as previously shown from SEM observations. In addition, it was previously shown that stress in obliquely sputter-deposited thin

films can be mainly compressive for deposition angles lower than a few tens degrees (deposition conditions close to the conventional deposition) since a dense microstructure is produced and is consistent with intense particle bombardment arising from sputtered atoms. Increasing the deposition angle, films become almost stress-free for glancing angles [34]. This is mainly attributed to the development of more tilted columns and increase of voids fraction between columns, because of shadowing effect and lower deposited energy. The transition from compact to highly porous films when deposition angle overpasses 60° and tends to 85°, also means that the grain boundaries density and growth defects inside the columns are largely increased.

DC electrical resistivity ρ as a function of temperature T was systematically measured from 7 to 300 K for the 9 studied metals and for deposition angle changing from 0 to 85° (to see Supplementary Material Section II for all studied transition metals). For films prepared with a conventional deposition angle ($\alpha = 0°$), a typical metallic-like behavior is obtained as shown as an example in Fig. 4 for Zr, Ta and Cr films. A linear evolution is observed from ρ *vs.* T measurements for temperatures down to a few tens of K for all metals, except for Cr where a clear saturation of resistivity appears as the temperature is higher than 150 K for $\alpha = 0°$ (Fig. 4c). This linear variation of ρ *vs.* T is commonly observed in nonmagnetic metallic crystalline materials. Such a temperature dependence of the electrical resistivity arises mainly from the electron-phonon interaction. Decreasing even more the temperature (typically, when it is lower than about 15 K) the metal resistivity becomes constant which defines the residual resistivity, namely ρ_o. The latter is essentially temperature independent and is due to electron scattering by defects.

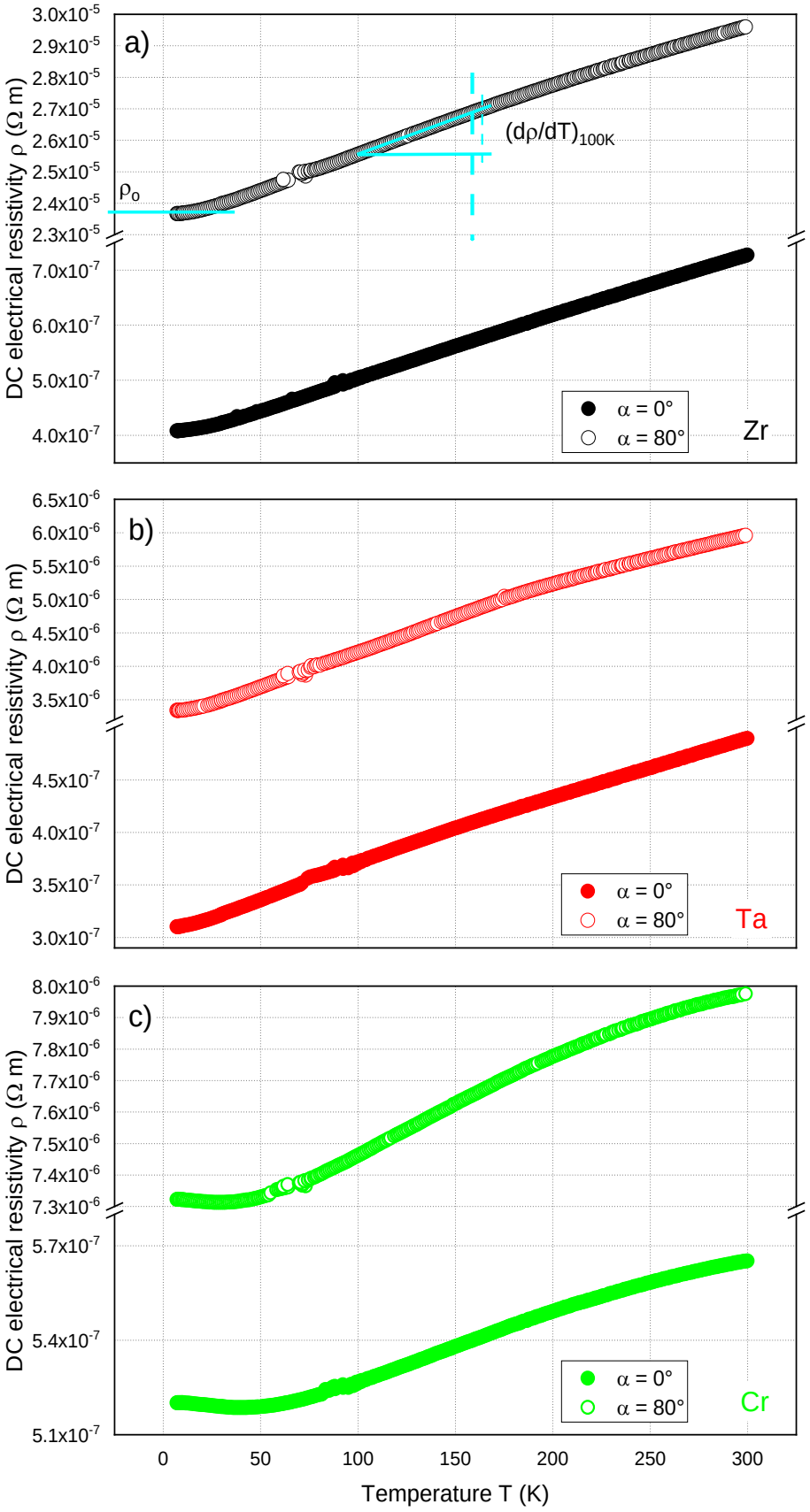
a)
b)
c)
DC electrical resistivity ρ (Ω m)
Temperature T (K)
ρo
(dρ/dT)100K
α = 0°
α = 80°
Zr
Ta
Cr
3.0x10-5
2.9x10-5
2.8x10-5
2.7x10-5
2.6x10-5
2.5x10-5
2.4x10-5
2.3x10-5
7.0x10-7
6.0x10-7
5.0x10-7
4.0x10-7
6.5x10-6
6.0x10-6
5.5x10-6
5.0x10-6
4.5x10-6
4.0x10-6
3.5x10-6
4.5x10-7
4.0x10-7
3.5x10-7
3.0x10-7
8.0x10-6
7.9x10-6
7.8x10-6
7.7x10-6
7.6x10-6
7.5x10-6
7.4x10-6
7.3x10-6
5.7x10-7
5.4x10-7
5.1x10-7
0
50
100
150
200
250
300

Figure 4: Some typical evolutions of DC electrical resistivity ρ vs. temperature T of a) Zr, b) Ta and c) Cr films prepared with a deposition angle α = 0° and 80°. The derivative of the resistivity by temperature at 100 K $(d\rho/dT)_{100K}$ and residual resistivity ρ_o are given for Zr film prepared with α = 80° as an example.

For all investigated metals, residual resistivity was measured at 7 K assuming that $\rho_o = \rho_{7K}$ and the linear dependency of resistivity was determined from the derivative at 100 K defined as $(d\rho/dT)_{100K}$ (Fig. 4a). As usual, films prepared with α = 0° are systematically more resistive than bulk metals (about one order of magnitude). The electron mean free path is reduced due to the small grain size commonly obtained in metallic thin films sputter-deposited at room temperature.

The large increase of resistivity is thoroughly obtained for the 9 transition metals prepared with a deposition angle higher than 60°. This enhancement of one to two orders of magnitude is clearly measured at any temperature when α changes from 0 to 80° and even more when the deposition angle reaches 85° (to see Supplementary Material Section II). Others have ever reported this effect for pure metals [38] and alloys [23, 24]. It has to be principally connected to the scattering mechanism of electrons, which is not only ruled out by phonons, but also by the disordering effect and defects becoming predominant as the deposition angle rises. At first, this enhanced electrical resistivity systematically measured as the deposition angle increases can be assigned to a decrease of the electron mean free path. GIXRD patterns (Fig. 2) showed a significant reduction of the grain size when the deposition angle is over than 60° (Fig. 3). Smaller grains lead to more scattering phenomena of free electrons at the ground boundary. Such a scattering favors the resistivity of metals, and in our films, it contributes to shift the overall ρ *vs.* T evolution to more resistive values. In addition, the high porous structure

induced by the atomic shadowing effect hinders the electron mean free path. The voided structure produces barriers for the electron path reducing their transport and thus increasing the resistivity. In the same way, this shadowing effect favors the sensitivity of the films to oxidation phenomenon (greater surface-to-volume ratios promote progressive oxygen enrichment and thus occurrence of the poorly conductive β-phase for some metals), which also contributes to the resistive character of the films.

For all deposition angles, resistivity of Cr films exhibits a saturation effect (a little for W, Ta, V and Nb films, and very lightly for Ti and Zr films, as shown in the Supplementary Material Section II) as the temperature tends to 300 K, which becomes more pronounced when the deposition angle increases (Fig. 4c). This nonlinear variation of ρ *vs.* T giving rise to a saturated resistivity has ever been observed for conventional metallic thin films and other alloys [39]. It is assigned to a strong reduction of the electron mean free path, which becomes in the order of the interatomic spacing due to structural disorder produced by alloying or defects [40]. Recent investigations from Sundqvist [41] interestingly suggested that this saturation phenomenon cannot be solely attributed to a single mechanism, but any scattering process that induces a sufficiently short electron state lifetime may cause resistivity saturation as well. The author pertinently showed that modifications of the classical Bloch-Grüneisen law (describing the electron-phonon interactions) produce very good agreement between theory and experiment. It well describes the temperature dependence of resistivity for many materials (single elements, intermetallic compounds, binary and ternary alloys, multi-component alloys and so on). However, there is no single and universal mechanism allowing a clear explanation of this saturation behavior. For our Cr thin films prepared with different deposition angles, the loss of long-range order combined to the increase of structural defects both contribute for reducing the electron mean free path and the electron-phonon interactions. However, this

saturation effect still remains an open question since it is clearly substantial for Cr films, a little noticeable for other metals like W, Ta, V or Nb, and very slightly measured or even missing for the other studied transition metals (to see the Supplementary Material Section II).

Around 50 K and for Cr films only, a minimum of resistivity can be noticed in the ρ *vs.* T measurements. Such a minimum was not observed for the other metallic films despite a more or less obvious saturation effect of the resistivity at high temperature. For some metallic systems containing very small amounts of ferromagnetic impurities, this kind of behavior is well known as the Kondo effect [42, 43]. Other mechanisms such as disorder-enhanced electron-electron interactions, weak localization, or spin-polarized tunneling through grain boundaries have been suggested for explaining this resistivity minimum in conventional thin films [23]. Due to the temperature range of the resistivity minimum (around 50 K), it corresponds to an unrealistic impurity concentration (more than a few at. %), which does not agree with the purity level obtained in a vacuum sputtering process involving a Cr target (purity higher than 99.9 at. %). Consequently, the Kondo effect can be first neglected for our GLAD Cr films. An electron-electron interaction seems to be more relevant assuming that this mechanism is favored in the low-temperature regime, particularly when the material becomes more disordered (as progressively observed for GLAD films prepared with an increasing deposition angle). This kind of interaction takes form through a square root temperature dependence of the resistivity [44], as successfully fitted for all Cr films prepared with different deposition angles ($\Delta\rho = \rho - \rho_{min}$ *vs.* $T^{1/2}$ shown in the Supplementary Material Section IV). In addition, the extracted coefficient β (Al'tshuler's parameter) varies linearly with $\rho_{min}^{5/2}$, which supports that the low-temperature resistivity of Cr films well follows an electron-electron interaction [45].

From ρ *vs.* T measurements performed for all investigated transition metals, the residual resistivity ρ_{7K} and the derivative at 100 K $(d\rho/dT)_{100K}$ have been systematically determined as

a function of the deposition angle (for clarity, Cr, Ta and Zr films are only shown in Fig. 5a and b). Both parameters exhibit the same evolution as a function of the deposition angle, i.e., a slight increase up to $\alpha = 60°$, then a steeper rising for films prepared with α tending to the glancing angles. Again, this α value appears as a critical angle from which the growth of the films mainly depends on the surface shadowing mechanism. Whatever the metal, surface morphology, structure at the micro- and nanoscale and so the resulting properties of the films are systematically modified from this angle.

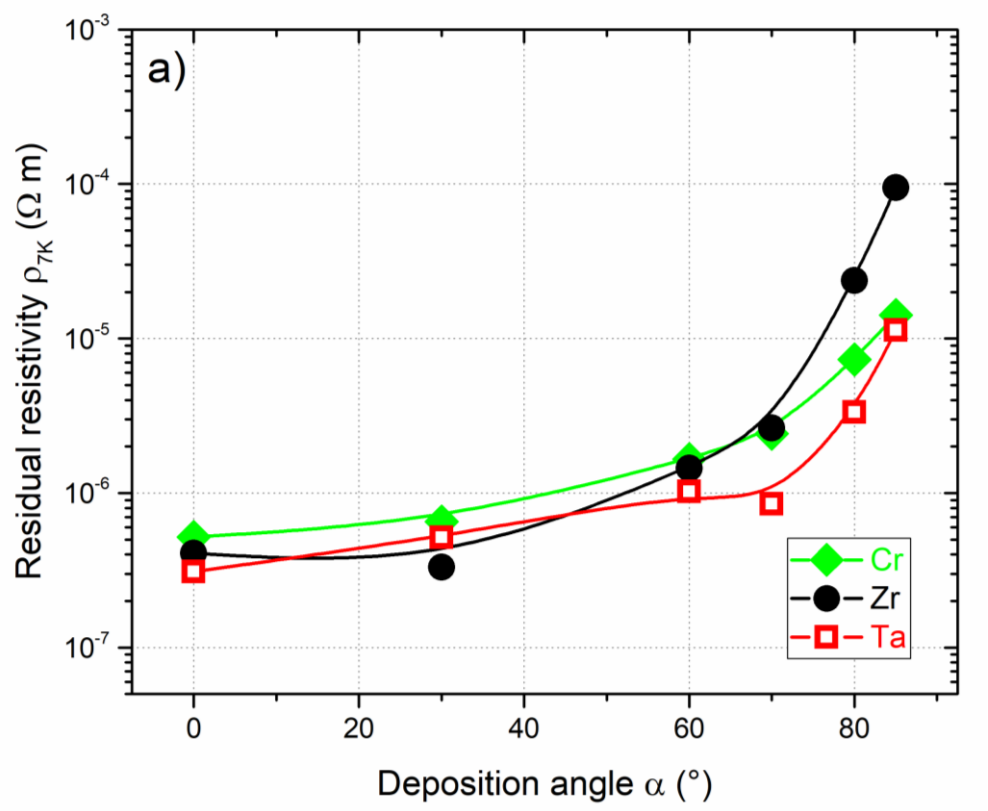

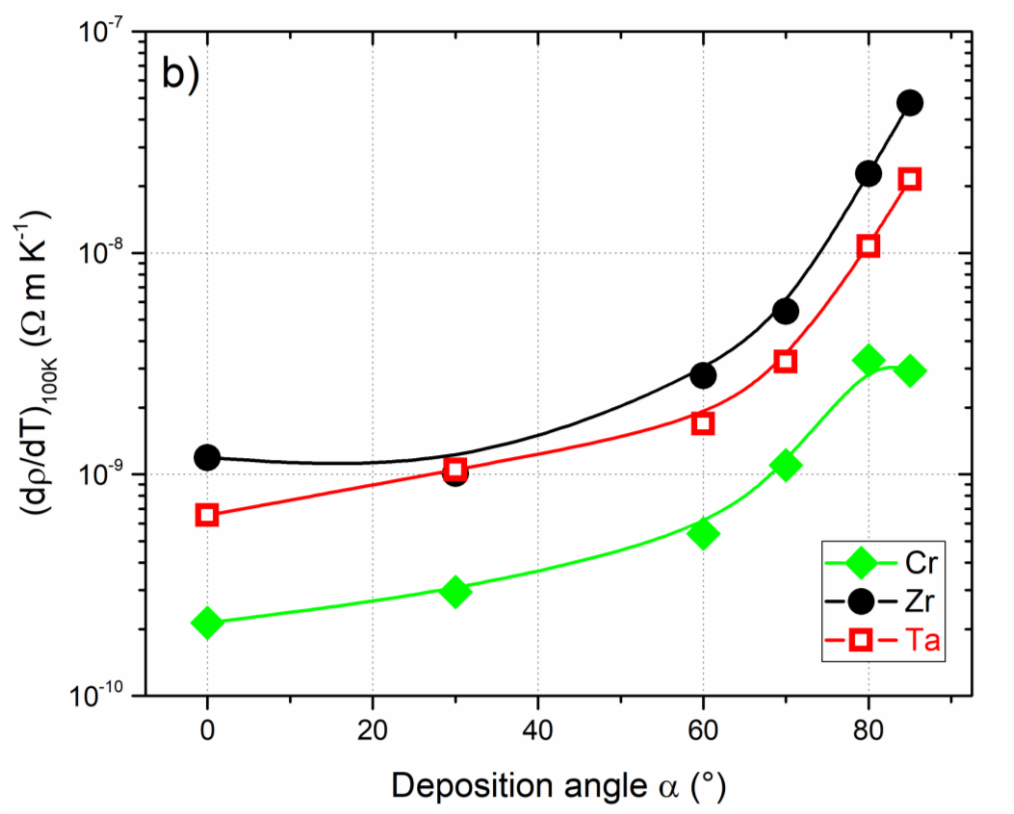

Figure 5: a) Residual resistivity obtained at 7 K (ρ_{7K}) and b) derivative of the resistivity by temperature at 100 K $(d\rho/dT)_{100K}$ as a function of the deposition angle α for Zr, Ta and Cr thin films sputter-deposited by oblique angle deposition (lines are a guide for the eye).

It is worth noting that residual resistivity spreads out over 2 to 3 orders of magnitudes when deposition angle changes from 0 to 85°. Since it is closely related to the concentration of impurities and crystallographic defects in the material, this strong increase of residual resistivity could be anticipated. Correspondingly, one can expect the same feature of the resistivity at room temperature as a function of the deposition angle (as successfully demonstrated and modeled by Besnard *et al.* [38]). The derivative at 100 K $(d\rho/dT)_{100K}$ similarly changes *vs.* α with a small increase until 60°, followed by an abrupt increase. This means that electrical conductivity of GLAD films prepared with the highest glancing angles become more sensitive to the temperature, and so the high-temperature resistivity is even more dominated by the electron-

phonon interaction. Such a phenomenon is illustrated by the Bloch-Grüneisen's law and requires further investigation to clarify the connection between electronic transport properties and structural disorder induced by the GLAD process (out of the scope of the paper).

Plotting derivative of the resistivity by temperature at 100 K $(d\rho/dT)_{100K}$ *vs.* residual resistivity obtained at 7 K (ρ_{7K}) clearly shows the influence of deposition angle on electron scattering by structural disorders and phonons (Fig. 6). Bulk values obtained from a classical database [46] are located in the part of the diagram corresponding to the lowest ρ_{7K} and $(d\rho/dT)_{100K}$. Their behaviors are expected since bulk materials are assumed as the purest single crystal with the lowest concentration of defects and impurities. They have to produce the longest electron mean free paths and the highest TCRs (Temperature Coefficient of Resistance). However, it is interesting to note that for bulk metals as well as films prepared with the lowest deposition angles, $(d\rho/dT)_{100K}$ values exhibit similar orders of magnitude, i.e., around 10^{-10} to 10^{-9} Ω m K^{-1}, whereas GLAD films systematically show higher residual resistivities. In addition, $(d\rho/dT)_{100K}$ values are lower than the MIR (Mott-Ioffe-Regel) limit as expected for simple metals and conventional metallic thin films (around 10^{-8} Ω m K^{-1} from [47]). As previously reported, high deposition angles produce structural disorders and reduce the crystal size, which both favor a strong electron scattering. Even at very low temperature, GLAD films prepared with the highest deposition angles exhibit resistivity beyond the MIR limit and residual resistivity close to 10^{-5} Ω m or even higher, leading them to be classified as "bad" metals [46].

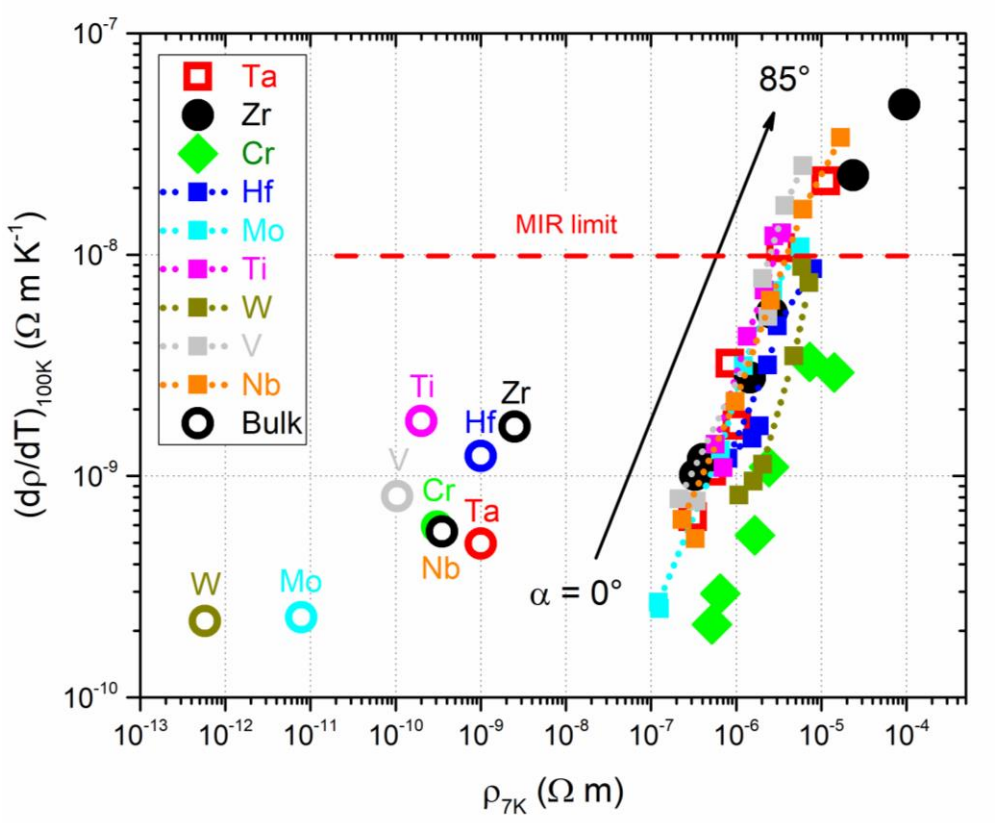

Figure 6: Derivative of the resistivity by temperature at 100 K $(d\rho/dT)_{100K}$ vs. residual resistivity obtained at 7 K (ρ_{7K}) for the 9 transition metals sputter-deposited with an increasing deposition angle α from 0 to 85°. Bulk values obtained from [46] are also indicated (open circles). The MIR (Mott-Ioffe-Regel) limit [47] is indicated (red dashed line).

By plotting with Log scales $(d\rho/dT)_{100K}$ *vs.* ρ_{7K}, a linear increase is clearly obtained as the deposition angle changes from α = 0 to 85° for all 9 GLAD thin films. Guo *et al.* [47] similarly reported the same trend for various metallic glasses assuming the linear coefficient of temperature *vs.* room-temperature resistivity. Although they showed a saturation value of the T-linear resistivity coefficient close to 10^{-8} Ω m K^{-1} (MIR limit) for all their studied systems, overcoming it cannot completely excluded, especially for GLAD films prepared with α > 70° where defects and structural disorders particularly increase leading to a strong electron

scattering and so a high slope of ρ(T). Boekelheide *et al.* [48] similarly reported that dρ/dT increases proportionally to the residual resistivity. Due to grain boundaries, valleys between columnar grains and voids, potential barriers are produced and electrons take a longer and tortuous path through the film. This geometry effect induces a change in the effective length of the sample. The authors also reported that for Cr films, the resistivity *vs.* temperature evolution is more complex than a conventional Matthiessen's rule and multiple temperature-dependent effects have to be assumed.

In order to further understand the effect of deposition angle on the scattering mechanism of electrons in GLAD thin films, resistivity *vs.* temperature measurements have been deeper investigated for the 9 metals. To this aim, the electron-phonon-defect interference has been analyzed by focusing evolution of resistivity in the temperature range around $0.1\times\theta_D$, i.e., in-between 7-100 K. For the lowest temperature reached with our experimental setup (i.e., around 7K), it is well below the temperature range imposed by Ta (the smallest Debye temperature of the 9 studied metals leads to $0.1\times240 = 24$K). It is also worth noting that ρ *vs.* T measurements (To see Supplementary Material Section II) all exhibit a clear temperature invariant resistivity for temperatures lower than 10K, which clear defines the residual resistivity. When the temperature is over $0.1\times\theta_D$ and around 100K, all metals show the typical ρ *vs.* T linear variation. This temperature range corresponds to the electron-phonon interaction. Assuming the intersection between $(d\rho/dT)_{100K}$ and ρ_{7K}, (or the lowest resistivity value for Cr films), a crossover temperature, namely T_{Cr}, can be determined for all studied metal films and as a function of the deposition angle. Three examples are given in figure 7 for Cr films prepared with α = 0, 30 and 85°. For such Cr films, ρ *vs.* T measurements well illustrate the different electron scattering mechanisms possible in disordered metallic compounds.

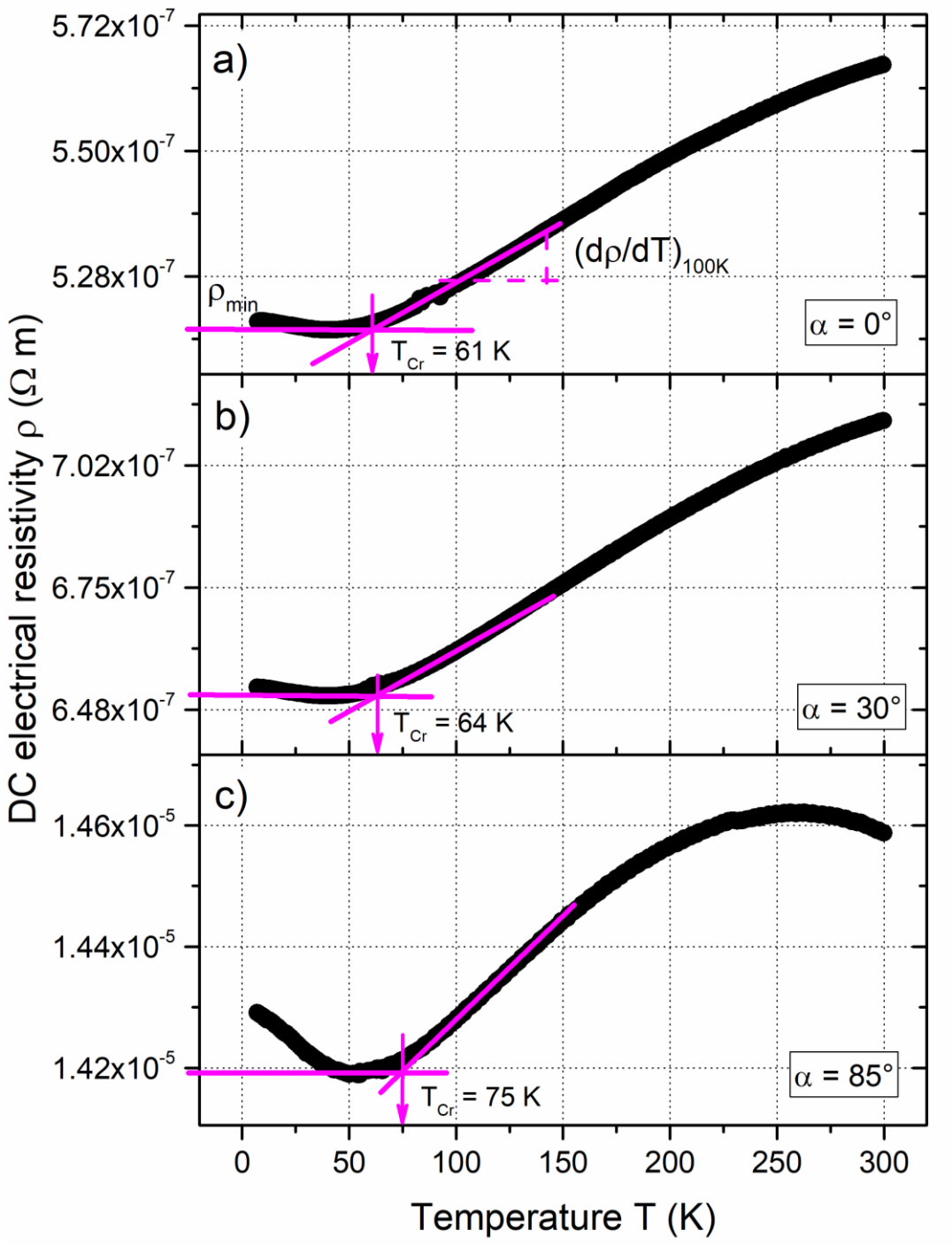

Figure 7: Resistivity vs. temperature of Cr films prepared at 3 deposition angles. The crossover temperature T_{Cr} representing the transition from T-linear to T^5 behavior is determined assuming the intersection between the residual resistivity (minimum resistivity value ρ_{min} for Cr films and from ρ_{7K} for the other metals), and the derivative of the resistivity by temperature at 100 K, $(d\rho/dT)_{100K}$.

Although the minimum of the resistivity (due to electron-electron interaction) and saturation effect (coming from disordering) are scarcely discernable for films prepared with the lowest deposition angles (Fig. 7a and 7b), they become more and more significant increasing α and a maximum of resistivity can be even noticed at 260 K for α = 85° (Fig. 7c). This unusual behavior in single metallic compounds, but rather encountered in many binary and ternary alloys, supports again the analysis proposed by Mooij where the electron mean free path tends to a lower limit corresponding to the shortest interatomic distance [41, 49]. As a result, the high scattering of electrons in these strongly disordered materials (possible s-d scatters) and the increase of the concentration of conduction electrons with temperature both favor the occurrence of a resistivity maximum at high temperature.

The temperature dependences of resistivity for impure and defective metals strongly differ from those of clean metals. Based-on previous works from Ptitsina *et al.* [50], it is worth determining the crossover temperature (T_{Cr}). The latter is defined as the temperature where two electron scattering processes compete to each other: the "pure" electron-phonon scattering commonly described by the Bloch-Grüneisen law (with a linear temperature dependence), and the inelastic electron scattering from impurities (such as defects, boundaries, and so on) corresponding to a constant resistivity at low temperature (and ultimately tending to the residual resistivity). The transition between these two scattering processes gives rise to electron-phonon-defect mechanisms at temperatures around $0.1\times\theta$, where θ is the Debye temperature with a T^5 dependence of the resistivity. For the 9 investigated transition metal thin films, resistivity *vs.* temperature was systematically measured for all deposition angles (to see the Supplementary Material Section II). An emphasis was put on the two opposite deposition angles (i.e., α = 0 and 85°) for getting the crossover temperature from $(d\rho/dT)_{100K}$ and ρ_{7K}, (or the lowest resistivity

value for Cr films). For each metal and for these two angles, T_{Cr} can be compared to θ, as shown in figure 8. For all metallic films prepared by conventional sputtering (α = 0°), the crossover temperature determined for each metal clearly exhibits a linear evolution as a function of the corresponding Debye temperature with a slope of 0.11. Such a slope agrees well with the temperature range theoretically and experimentally reported (i.e., T ≈ 0.1×θ) in metals, which correlates with the interference between electron-phonon and electron-defect scattering [51-53].

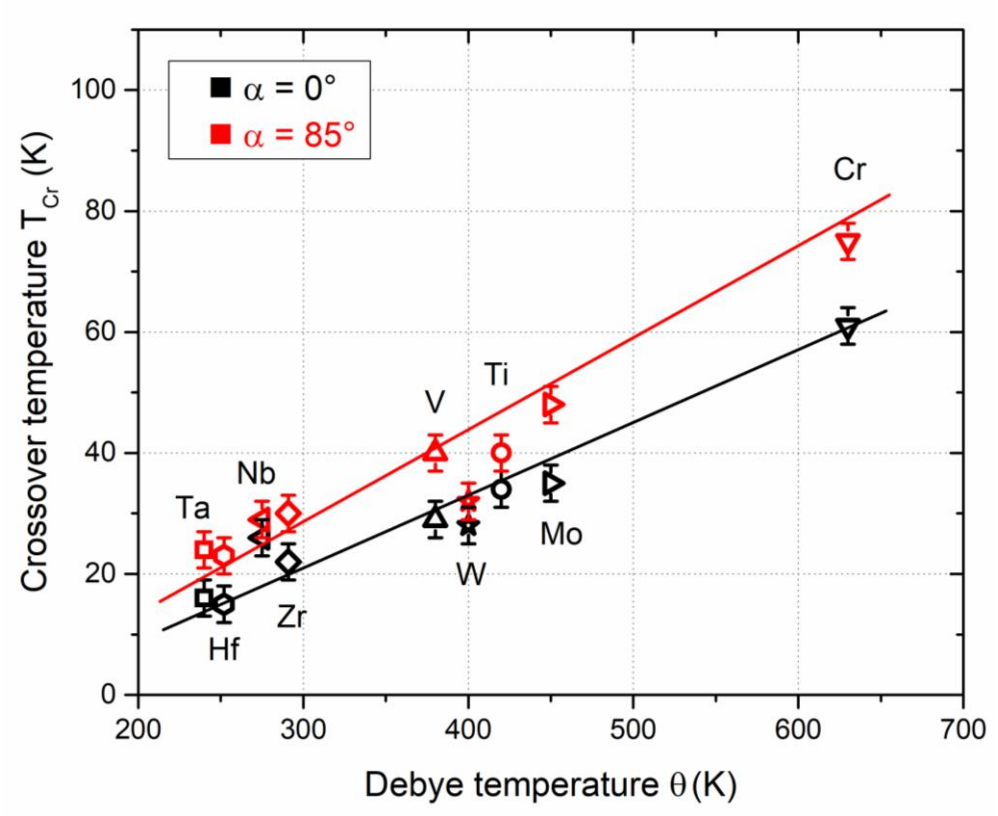

Figure 8: Crossover temperature T_{Cr} from linear to T^5 behavior (electron-phonon-defect interference) as a function of the Debye temperature θ for hcp and bcc transition metals and for two deposition angles α = 0 and 85°. A linear fit of T_{Cr} vs. θ gives rise to a slope of 0.11 (black line) and 0.15 (red line) for α = 0 and 85°, respectively.

Increasing the deposition angle and particularly for the films prepared with $\alpha = 85°$, the crossover temperature is systematically shifted to higher temperatures for all metals, as illustrated in Fig. 8. This means that in the electron-phonon-defect interference phenomenon, the effect of defects on electron scattering predominates for a wider range of temperatures. This temperature shift correlates with the rising concentration of structural defects and the lowering of crystal size (Fig. 3) when the deposition angle tends to be more and more glancing. Assuming investigation from Ptitsina *et al.* [50] focused on electronic transport in disordered metals, the crossover temperature at which each interaction (electron-defect and electron -phonon) similarly contributes to electron scattering, strongly depends on the electron mean free path and on the longitudinal-to-transverse sound velocity ratio.

However, the authors also suggested that other physical mechanisms have to be taken into account for understanding electron scattering and thus variations of the crossover temperature. As a result, this temperature shift systematically measured for films prepared with the highest deposition angles can also be correlated with the anisotropic behavior of the columnar microstructure especially produced by means of the GLAD growth [54]. When deposition angles reach glancing values (i.e., $\alpha > 70°$), columns with an elliptical cross section can be produced for metals leading to a preferential growth of the columnar structure in the direction perpendicular to the particle flux [36, 55]. This morphological asymmetry of the columnar structure may also induce an anisotropy of the electron motion, and so an effect on the electron mean free path.

In the same way, it is worth noticing that the T_{Cr} *vs.* θ interpolation gives rise to a higher slope for GLAD films, i.e., slope = 0.11 for conventional films whereas it is higher than 0.15 for $\alpha = 85°$. For all metals and assuming the results shown in figure 6, both residual resistivity ρ_{7K} as well as $d\rho/dT$ increase as a function of the deposition angle (about 3 orders of magnitude

as α changes from 0 to 85°). Jäckle and Froböse [56] and later others [57] reported that the slope dρ/dT is proportional to the transport electron-phonon coupling constant with a coefficient depending on multiple effects (nano-structure, grain boundaries, electron-phonon coupling, electron concentration at the Fermi energy [48]). It is not obvious, therefore, to clearly prove which physical mechanism prevails and impacts on the value of the crossover temperature, although structural disorder in the columnar architecture strongly influences electron mean free path and so the electron-phonon-defect interference.

4. Conclusions

Thin films of 9 transition metals (Ti, V, Cr, Zr, Nb, Mo, Hf, Ta, W) were sputter-deposited by the oblique angle deposition process. The deposition angle α was systematically and gradually changed from 0 to 85°. It was found that the tilted columnar architecture is enhanced when α rises, leading not only to a more voided and disordered structure, but also to a reduction of the crystal size. Measurements of resistivity ρ as a function of the temperature T in between 7–300 K showed a typical metallic-like behavior for films prepared by conventional sputtering (α = 0°).

Increasing the deposition angle gives rise to more resistive films with a residual resistivity tending to be higher than 10^{-5} Ω m for all films prepared at a deposition angle α = 85°. At low temperature, electron scattering by defects and impurities prevails and is enhanced because high deposition angles favor structural defects and porosity between and inside the tilted columns. For temperatures higher than 100 K, the electron-phonon interaction predominates corresponding to a typical linear dependence of ρ *vs.* T, and $(d\rho/dT)_{100K}$ progressively increases as the deposition angle tends to glancing values.

From resistivity measurements, the electron-defect scattering phenomenon was clearly illustrated at low temperature, whereas the electron-phonon interaction was obtained for high temperature. The crossover temperature T_{Cr} corresponding to the competition between these two electron scattering processes (electron-defect-phonon interference effect) was related to the Debye temperature θ with a typical behavior for conventional films (i.e., T_{Cr} in the range of $0.1\times\theta$). Depositing with higher angles ($\alpha > 60°$) produced a more voided and tilted columnar architecture with more structural defects. Residual resistivity as well as $(d\rho/dT)_{100K}$ both increased as a function of the deposition angle (3 orders of magnitude from $\alpha = 0$ to 85°), and similarly the crossover temperature was shifted to higher temperature with $T_{Cr} = 0.15\times\theta$, supporting that disorder and voids in the columnar architecture strongly influence electron scattering mechanisms.

CRediT authorship contribution statement

Hamidreza Gerami: Data curation; Validation; Writing - review & editing. **Jean-Marc Cote:** Data curation; Software; Writing - review & editing. **Antonio Jesús Santos:** Writing - review & editing. **Nicolas Martin:** Writing - review & editing; Supervision; Funding acquisition.

All authors have read and agreed to the published version of the manuscript.

Declaration of Competing Interest

The authors declare that they have no known competing financial interests or personal relationships that could have appeared to influence the work reported in this paper.

Data availability

Data will be made available on request.

Acknowledgements

This work has been achieved in the frame of the EIPHI Graduate school (contract "ANR-17-EURE-0002" and by the Bourgogne-Franche-Comté Region. It has also been partly supported by the French RENATECH network and its FEMTO-ST technological facility. A. J. Santos would like to thank the University of Cádiz and the Spanish Ministerio de Universidades for the concession of a "Margarita Salas" postdoctoral fellowship funded by the European Union - NextGenerationEU (2021-067#9663/PN/MS-RECUAL/CD).

Appendix A: Supplementary data

Supplementary Material to this article can be found on line at https:// …

References

[1] P. Wissman, H.U. Finzel, Electrical resistivity of thin metal films, Springer, Heidlberg, 2007, https://doi.org/10.1007/3-540-48490-6

[2] P.L. Rossiter, The electrical resistivity of metals and alloys, Cambridge University Press, Cambridge, 1987, https://doi.org/10.1017/cbo9780511600289

[3] C.R. Tellier, A.J. Tosser, Size effects in thin films, Elsevier Scientific Publishing Company, Amsterdam, 1982, https://doi.org/10.1016/c2009-0-12632-6

[4] E.M. Gershenzon, M.E. Gershenzon, G. N. Gol'tsman, A. M. Lyul'kin, A. D. Sernenov, A.V. Sergeev, Electron-phonon interaction in ultrathin Nb films, Sov. Phys. JEPT 70 (1990) 505-511.

[5] A. Sergeev, B.S. Karasik, M.E. Gershenson, V. Mitin, Electron–phonon scattering in disordered metallic films, Physica B 316-317 (2002) 328-330, https://doi.org/10.1016/s0921-4526(02)00499-4

[6] J.J. Lin, C.Y. Wu, Electron-phonon scattering time in crystalline disordered $Ti_{1-x}Al_x$ alloys, Physica B 219-220 (1996) 68-70, https://doi.org/10.1016/0921-4526(95)00652-4

[7] K.S. Ll'in, N.G. Ptitisna, A.V. Sergeev, G.N. Gol'tsamn, E.M. Gershenzon, B.S. Karasik, Interrelation of resistivity and inelastic electron-phonon scattering rate in impure NbC films, Phys. Rev. B 57 (1998) 15623-6, https://doi.org/10.1103/physrevb.57.15623

[8] N.G. Ptitsina, G.M. Chulkova, E.M. Gershenzon, M.E. Gershenzon, Influence of the interface of electron-phonon and electron-impurity scattering on the conductivity of unordered Nb films, JETP 80 (1995) 960-964.

[9] T. Sun, B. Yao, A.P. Warren, K. Barmak, M.F. Toney, R.E. Peale, K.R. Coffey, Dominant role of grain boundary scattering in the resistivity of nanometric Cu films, Phys. Rev. B 79 (2009) 0414402-4, https://doi.org/10.1103/physrevb.79.041402

[10] A.I. Oliva, J.M. Lugo, R.A. Gurubel-Gonzalez, R.J. Centeno, J.E. Corona, F. Avilès, Temperature coefficient of resistance and thermal expansion coefficient of 10-nm thick gold films, Thin Solid Films 623 (2017) 84-89, https://doi.org/10.1016/j.tsf.2016.12.028

[11] A.L. Lima, X. Zhang, A. Misra, C.H. Booth, E.D. Bauer, M.F. Hundley, Length scale effects on the electronic transport properties of nanometric Cu/Nb multilayers, Thin Solid Films 515 (2007) 3574-3579, https://doi.org/10.1016/j.tsf.2006.11.004

[12] C. Adelmann, On the extraction of resistivity and area of nanoscale interconnect lines by temperature-dependent resistance measurements, Solid State Electron. 152 (2019) 72-80, https://doi.org/10.1016/j.sse.2018.12.005

[13] D.K. Sharma, R. Srivastava, Negative temperature coefficient of resistivity in thin metallic wires, J. Mater. Sci. Lett. 2 (1983) 775-776, https://doi.org/10.1007/bf00720557

[14] H.D. Wang, J.H. Liu, X. Zhang, Z.Y. Guo, K. Takahashi, Experimental study on the influences of grain boundary scattering on the charge and heat transport in gold and platinum nanofilms, Heat Mass Transf. 47 (2011) 893-898, https://doi.org/10.1007/s00231-011-0825-5

[15] A. Barranco, A. Borras, A.R. Gonzalez-Elipe, A. Palmero, Perspectives on oblique angle deposition of thin films: From fundamentals to devices, Progr. Mater. Sci. 76 (2016) 59-153, https://doi.org/10.1016/j.pmatsci.2015.06.003

[16] M.M. Hawkeye, M.T. Taschuk, M.J. Brett, Glancing angle deposition of thin films: Engineering the nanoscale, John Wiley & Son Ltd, Chichester, 2014, https://doi.org/10.1002/9781118847510

[17] N. Martin, J.M. Cote, H. Boukhalfa, V. Potin, Checkerboard-like structure in columnar W-Mo thin films, Funct. Mater. Lett. 15 (2022) 2251043-5, https://doi.org/10.1142/s1793604722510432

[18] S. Hurand, A. Corvisier, B. Lacroix, A.J. Santos, F. Maudet, C. Dupeyrat, R.G. Roja, F.M. Morales, T. Girardeau, F. Paumier, Anisotropic optical properties of indium tin oxide thin films prepared by ion beam sputtering under oblique angle deposition, Appl. Surf. Sci. 595 (2022) 152945-11, https://doi.org/10.1016/j.apsusc.2022.152945

[19] N. Martin, J. Sauget, T. Nyberg, Anisotropic electrical resistivity during annealing of oriented columnar titanium films, Mater. Lett. 105 (2013) 20-23, https://doi.org/10.1016/j.matlet.2013.04.058

[20] T. Otiti, G.A. Niklasson, P. Svedlindh, C.G. Granqvist, Anistropic optical, magnetic and electrical properties pf obliquely evaporated Ni films, Thin Solid Films 307 (1997) 245-249, https://doi.org/10.1016/s0040-6090(97)00257-5

[21] M. Yang, K. Gao, P. Xing, T. Yi, Z. He, B. Ke, Microstructure and thermal stability of glance angle deposited Au nanofilms, Mater. Today Commun. 31 (2022) 103718-12, https://doi.org/10.1016/j.mtcomm.2022.103718

[22] A.M. Engwall, L.B. Bayu Aji, A.A. Baker, S.J. Shin J.H. Bae, S.K. McCall, J.M. Moody, S.O. Kucheyev, Effect of substrate tilt on sputter-deposited AuTa films, Appl. Surf. Sci. 547 (2021) 149010-7, https://doi.org/10.1016/j.apsusc.2021.149010

[23] Z. Ali, D. Basaula, W. Zhou, J. Brock, M. Khan, K.F. Eid, Controlling the charge transport mode in permalloy films using oblique angle deposition, J. Magn. Magn. Mater. 484 (2019) 430-436, https://doi.org/10.1016/j.jmmm.2019.03.087

[24] Z. Ali, D. Basaula, K.F. Eid, M. Khan, Anisotropic properties of oblique angle deposited permalloy thin films, Thin Solid Films 735 (2021) 138899-8, https://doi.org/10.1016/j.tsf.2021.138899

[25] A. Anders, A structure zone diagram including plasma-based deposition and ion etching, Thin Solid Films 518 (2010) 4087-4090, https://doi.org/10.1016/j.tsf.2009.10.145

[26] H. Boukhalfa, V. Potin, N. Martin, Ballistic and thermalized regimes to tune structure and conducting properties of W-Mo thin films, Vacuum 204 (2022) 111347-10, https://doi.org/10.1016/j.vacuum.2022.111347

[27] R. Mareus, C. Mastail, F. Nita, A. Michel, G. Abadias, Effect of temperature on the growth of TiN thin films by oblique angle sputter-deposition: A three-dimensional atomistic computational study, Comput. Mater. Sci. 197 (2021) 110662-12, https://doi.org/10.1016/j.commatsci.2021.110662

[28] R.F. Peart, J. Askill, The mechanism of diffusion in bcc transition metals, Phys. Stat. Sol. 23 (1967) 263-275, https://doi.org/10.1002/pssb.19670230126

[29] J. Peralta, J. Esteve, A. Lousa, δ-A15 and bcc phases coexist in sputtered chromium coatings with moderate oxygen contents, Thin Solid Films 693 (2020) 137676-7, https://doi.org/10.1016/j.tsf.2019.137676

[30] D.J. Poxson, F.W. Mont, M.F. Schubert, J.K. Kim, E.F. Schubert, Quantification of porosity and deposition rate of nanoporous films grown by oblique-angle deposition, Appl. Phys. Lett. 93 (2008) 101914-3, https://doi.org/10.1063/1.2981690

[31] A. Siad, A. Besnard, C. Nouveau, P. Jacquet, Critical angles in DC magnetron GLAD thin films, Vacuum 131 (2016) 305-311, https://doi.org/10.1016/j.vacuum.2016.07.012

[32] A.J. Santos, B. Lacroix, F. Maudet, A. Corvisier, F. Paumier, C. Dupeyrat, T. Girardeau, R. Garcia, F.M. Morales, Surface oxidation of amorphous Si and Ge slanted columnar and mesoporous thin films: Evidence, scrutiny and limitations for infrared optics, Appl. Surf. Sci. 493 (2019) 807-817, https://doi.org/10.1016/j.apsusc.2019.07.064

[33] A. van der Drift, Evolutionary selection, a principle governing orientation, Philips, Res. Rep. 22 (1967) 267-288.

[34] G. Abadias, F. Angay, R. Mareus, C. Maistal, Texture and stress evolution in HfN films sputter-deposited at oblique angles, Coatings 9 (2019) 712-15, https://doi.org/10.3390/coatings9110712

[35] S. Mahieu, P. Ghekiere, D. Depla, R. De Gryse, O.I. Lebedev, G. van Tendeloo, Mechanism of in-plane alignment in magnetron sputtered biaxially aligned yttria-stabilized zirconia, J. Crystal Growth 290 (2006) 272-279, https://doi.org/10.1016/j.jcrysgro.2005.12.093

[36] R. El Beainou, A. Chargui, P. Pedrosa, A. Mosset, S. Euphrasie, P. Vairac, N. Martin, Electrical resistivity and elastic wave propagation anisotropy in glancing angle deposited tungsten and gold thin films, Appl. Surf. Sci. 475 (2019) 606-514, https://doi.org/10.1016/j.apsusc.2019.01.041

[37] A. Singh, A. Sharma, M. Tomar, V. Gupta, Tunable nanostructured columnar growth of SnO_2 for efficient detection of CO gas, Nanotechnology 29 (2018) 065502-12, https://doi.org/10.1088/1361-6528/aa9bc0

[38] A. Besnard, N. Martin, L. Carpentier, B. Gallas, A theoretical model for the electrical properties of chromium thin films sputter deposited at oblique incidence, J. Phys. D: Appl. Phys. 44 (2011) 2015301-8, https://doi.org/10.1088/0022-3727/44/21/215301

[39] E.F. Talantsev, The electron-phonon coupling constant and the Debye temperature in polyhydrides of thorium, hexadeuteride of yttrium, and metallic hydrogen phase III, J. Appl. Phys. 130 (2021) 195901-13, https://doi.org/10.1063/5.0065003

[40] Z. Fisk, G.W. Webb, Saturation of the high-temperature normal-state electrical resistivity of superconductors, Phys. Rev. Lett. 36(18) (1976) 1084-186, https://doi.org/10.1103/physrevlett.36.1084

[41] B. Sundqvist, Resistivity saturation in crystalline metals: Semi-classical theory versus experiments, J. Physic. Chem. Solids 165 (2022) 110686-9, https://doi.org/10.1016/j.jpcs.2022.110686

[42] J. Kondo, Resistance minimum in dilute magnetic alloys, Progr. Theor. Phys. 32 (1964)-37-49, https://doi.org/10.1143/ptp.32.37

[43] P.K. Leung, J. Slechta, J.G. Wright, Kondo effect in structurally disordered single element magnetic materials, J. Phys. F: Metal. Phys. 4 (1974) L21-L23, https://doi.org/10.1088/0305-4608/4/2/004

[44] A. Jayakumar, V. Dixit, S. Jose, V.B. Kamble, D. Jaiswal-Nagar, Charge transport variation from Bloch-Grüneisen to Mott variable range hopping and transport change due to hydrogenation in palladium thin films, Sci. Rep. 11 (2021) 22298-18, https://doi.org/10.1038/s41598-021-01787-1

[45] Z. Li, Y. He, L. Jin, X. Li, B. Luo, Y. Zeng, M. Zhou, J. Zhang, Resistivity minimum in beryllium films, Phys. Status Solidi B 259 (2022) 2100335-7, https://doi.org/10.1002/pssb.202100335

[46] D.R. Lide (Ed.), CRC Handbook of Chemistry and Physics, Internet Version, 2005, CRC Press, Boca Raton, FL, 2005 (<http://www.hbcpnetbase.com>).

[47] Q. Guo, C. Magen, M.J. Rozenberg, B. Noheda, Phenomenological classification of metals based on resistivity, Phys. Rev. B 106 (2022) 085141-6, https://doi.org/10.1103/physrevb.106.085141

[48] Z. Boekelheide, D.W. Cooke, E. Helgren F. Hellman, Resonant impurity scattering and electron-phonon scattering in the electrical resistivity of Cr thin films, Phys. Rev. B 80 (2006) 134426-12, https://doi.org/10.1103/physrevb.80.134426

[49] J.H. Mooij, Electrical conduction in concentrated disordered transition metal alloys, Phys. Stat. Sol. (a) 17 (1973) 521-530, https://doi.org/10.1002/pssa.2210170217

[50] N.G. Ptitsina, G.M. Chulkova, K.S. Il'in, A.V. Sergeev, F.S. Pochinkov, E.M. Gershenzon, M.E. Gershenzon, Electron-phonon interaction in disordered metal films: The resistivity and electron dephasing rate, Phys. Rev. B 56(16) (1997) 10089-10096, https://doi.org/10.1103/physrevb.56.10089

[51] S.S. Yeh, J.J. Lin, J. Xiunian, Z. Dianlin, Electron-phonon-impurity interference effect in disordered $Au_{56}Pd_{44}$ and IrO_2 thick films, Phys. Rev. B 72 (2005) 024204-5, https://doi.org/10.1103/physrevb.72.024204

[52] M.Y. Reizer, A.V. Sergeev, The effect of the electron-phonon interaction of the conductivity of impure metals, Sov. Phys. JETP 65(6) (1987) 1291-1298.

[53] G. Claudio, R. Mauro, P. Chiara, M. Eugenio, R.M. Luisa, Study of disorder effect on titanium films resistivity, Physica B 329-333 (2003) 1533-1535, https://doi.org/10.1016/s0921-4526(02)02277-9

[54] D. Vick, T. Smy, M.J. Brett, Growth behavior of evaporated porous thin films, J. Mater. Res. 17 (11) (2002) 2904–2911, https://doi.org/10.1557/jmr.2002.0421

[55] A. Chargui, R. El Beainou, A. Mosset, J. Gavoille, P. Vairac, S. Euphrasie, N. Martin, Anisotropic thermal conductivity of nanocolumnar W thin films, Phys. Lett. A 426 (2022) 127878-4, https://doi.org/10.1016/j.physleta.2021.127878

[56] J. Jäckle, K. Froböse, The electron phonon coupling constant of amorphous metals, J. Phys. F: Metal Phys. 10 (1980) 471-476, https://doi.org/10.1051/jphyscol:19808127

[57] O. Rapp, J. Jäckle, K. Froböse, Relation between electron phonon coupling constant and resistivity of amorphous transition metal alloys, J. Phys. F: Metal Phys. 11 (1982) 2359-66, https://doi.org/10.1088/0305-4608/11/11/016

Figure captions

Figure 1

Top and cross-section SEM views of Zr, Ta and Cr films sputter-deposited: a), b) and c) by conventional sputtering ($\alpha = 0°$); d), e) and f) by oblique angle deposition with a deposition angle $\alpha = 80°$. White arrows indicate the direction of the incoming particle flux. The column angle β is also specified for the tilted columnar architectures.

Figure 2

Grazing incidence X-ray diffraction patterns of Zr, Ta and Cr films prepared a) by conventional sputtering ($\alpha = 0°$), and b) by oblique angle deposition with a deposition angle $\alpha = 80°$. ● = hcp Zr phase; ◘ = bcc α-Ta phase; ■ = A15 β-Ta phase; ◆ = bcc Cr phase.

Figure 3

Evolution of the crystal size L (Scherrer's law applied for the most intense peak obtained from XRD patterns) as a function of the deposition angle α for Zr, Ta and Cr films.

Figure 4

Some typical evolutions of DC electrical resistivity ρ vs. temperature T of a) Zr, b) Ta and c) Cr films prepared with a deposition angle $\alpha = 0°$ and 80°. The derivative of the resistivity by temperature at 100 K $(d\rho/dT)_{100K}$ and residual resistivity ρ_o are given for Zr film prepared with $\alpha = 80°$ as an example.

Figure 5

a) Residual resistivity obtained at 7 K (ρ_{7K}) and b) derivative of the resistivity by temperature at 100 K $(d\rho/dT)_{100K}$ as a function of the deposition angle α for Zr, Ta and Cr thin films sputter-deposited by oblique angle deposition (lines are a guide for the eye).

Figure 6

Derivative of the resistivity by temperature at 100 K $(d\rho/dT)_{100K}$ vs. residual resistivity obtained at 7 K (ρ_{7K}) for the 9 transition metals sputter-deposited with an increasing deposition angle α from 0 to 85°. Bulk values obtained from [46] are also indicated (open circles). The MIR (Mott-Ioffe-Regel) limit [47] is indicated (red dashed line).

Figure 7

Resistivity vs. temperature of Cr films prepared at 3 deposition angles. The crossover temperature T_{Cr} representing the transition from T-linear to T^5 behavior is determined assuming the intersection between the residual resistivity (minimum resistivity value ρ_{min} for Cr films and from ρ_{7K} for the other metals), and the derivative of the resistivity by temperature at 100 K, $(d\rho/dT)_{100K}$.

Figure 8

Crossover temperature T_{Cr} from linear to T^5 behavior (electron-phonon-defect interference) as a function of the Debye temperature θ for hcp and bcc transition metals and for two deposition angles α = 0 and 85°. A linear fit of T_{Cr} vs. θ gives rise to a slope of 0.11 (black line) and 0.15 (red line) for α = 0 and 85°, respectively.